Hindawi
International Journal of Photoenergy
Volume 2020, Article ID 7872916, 10 pages
https://doi.org/10.1155/2020/7872916

*Research Article*

# L vs. LCL Filter for Photovoltaic Grid-Connected Inverter: A Reliability Study

**Ignacio Villanueva,[1] Nimrod Vázquez,[1] Joaquín Vaquero,[2] Claudia Hernández,[1] Héctor López,[1] and Rene Osorio[3]**

[1]*Electronics Engineering Department, Tecnologico Nacional de Mexico - IT Celaya, 38010 Celaya, Guanajuato, Mexico*
[2]*Electronics Technology Area, Universidad Rey Juan Carlos, 28933 Mostoles, Madrid, Spain*
[3]*Computer Science and Engineering Department, University of Guadalajara, 46600 Ameca, Jalisco, Mexico*

Correspondence should be addressed to Nimrod Vázquez; n.vazquez@ieee.org

Received 17 October 2019; Accepted 4 January 2020; Published 29 January 2020

Guest Editor: Johnny P. Contreras



The increasing use of photovoltaic systems entails the use of new technologies to improve the efficiency and power quality of the grid. System performance is constantly increasing, but its reliability decreases due to factors such as the uncontrolled operation, the quality of the design and quantity of components, and the use of nonlinear loads that may lead to distortion in the signal, which directly affects the life of the system globally. This article presents an analysis of the reliability of a single-phase full-bridge inverter for active power injection into the grid, which considers the inverter stage with its coupling stage. A comparison between an L filter and an LCL filter, which comprise the coupling stage, is made. Reliability prediction is based on metrics, failure rate, mean time between failures, and total harmonic distortion. The analysis and numerical simulation are performed. Finally, filter considerations are suggested to extend the reliability of the inverter in a photovoltaic system.

## 1. Introduction

Nowadays exists a global concern about the excessive use of fossil energies and the environmental conditions caused by them. In recent years, global demand for electric energy has been constantly increasing, giving the opportunity for environmentally friendly energy alternatives, commonly known as renewable energy, for example, wind and solar energy; this last one is the most important due to solar irradiation on the planet [1, 2].

The photovoltaic systems have different stages of energy conversion and coupling to the electric grid, being complex and robust systems due to the big number of power semiconductors that are used [2]. The power converters are one of the weakest stages in terms of the useful life of photovoltaic systems; generally, a photovoltaic panel has a useful life in terms of reliability of 20 to 30 years, and the inverter is required to have a comparable useful life [3, 4]. This problem has been corrected replacing the inverter when it is needed, but economically is not viable, and the repair tends to be complex; this has carried to the search for solutions to extend the life of the system as a whole [4].

For the conversion stage, different factors influence the longevity and reliability of the inverters, such as the operating ranges, the operating environment, functioning temperature, and working times. All these directly affect the useful life of the semiconductor elements and the whole photovoltaic system [5]. The most susceptible device to fail is the MOSFET, presenting two fault states: open circuit and short circuit; another element is the diode, which is affected by electrical and thermomechanical stress. To correct these problems, materials, such as silicon carbide, are used, because of their higher voltage operating limits and lower switching losses. Also, cooling techniques and system designs are taking into account the conditions and the operating environment [6, 7].

Photovoltaic system performance may be affected for different aspects, such as deterioration of the waveforms causing harmonics and, therefore, reducing the power factor due to nonlinear loads. This is already being studied using control techniques with active or passive components for the grid injection stage [8]. Passive filters also affect the performance; they are conformed by components like inductors and capacitors. These filters have the main disadvantage in their size that may generate resonance problems if they work below the cutoff frequency. However, they present a small number of elements and are more robust [9].

Previous studies present strategies for the selection and improvement of the reliability of the converter. The authors in [7, 10, 11] propose to implement fault-tolerant converters; they perform diverse tests and compare results to different prototypes of the same converter. Some other authors, like in [4, 12], perform the analysis following the traditional method at the component level and, later, at the system level. The MIL HDBK 217 standard is used and a hybrid model for the calculation of the mean time between failure metrics. The research in [7, 13] focuses on methods based on the mission profile of the system, considering different active and inactive work phases at different temperature conditions observed by the system. Researches in [3, 14] represent systems analytically by means of logic gates and fault tree or "pareto" analysis considering a voltage component failure. Finally, in [15, 16], the Markov model is used for repairable systems using different failure and repair modes. All these previous works did not focus on the coupling stage, the passive filter, which certainly will affect the reliability of the photovoltaic system.

In this paper, a reliability study of a photovoltaic inverter is made to analyze and predict its useful life based on the probability of failures occurrences. The MIL HDBK 217F standard is used and a simulation is performed using the PSIM simulation software. The system is comprised of a full-bridge inverter, with an L or an LCL filter as the coupling stage; the objective is to determine which filter is recommended to extend the reliability and useful life of the system. Simulation results are presented as well as the system analysis using the standard mentioned before. A discussion based on the filter is made to improve the reliability of the photovoltaic system.

The document is organized as follows: first, a theoretical part is addressed, like reliability concept and the reliability standard; second, the power stage is addressed and the reliability analysis; as the third point, the simulation and discussion of proposals are made; and as the last part, the conclusions are presented.

## 2. Theoretical Aspects

To understand the analysis and proposal, some theoretical aspects are addressed first, but there are also some assumptions.

*2.1. Reliability.* Reliability describes the probability of survival of different complex electronic systems and is defined as the property that a component has to satisfactorily perform its function for which it was designed, for a specific time, under specific experimental conditions [6, 7]. Reliability is represented as $R(t)$ and given by

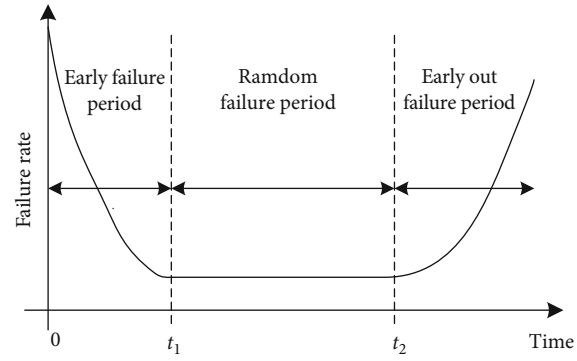


Figure 1: Typical risk ratio curve (bathtub).

$$R(t) = P(T > t) = 1 - F(t) = \int_0^t f(t)dt, \tag{1}$$

where $f(t)$ is a failure density function, $t$ is the time that the component will fail, $F(t)$ is the cumulative distribution function, and $P$ is the probability function.

The reliability is represented as the value that reaches the random variable $R$ in $t\epsilon[0, \infty]$; this is the area under the density function curve, which determines the probability that the component will fail at specific time $t$.

When an electronic component presents a risk, it is called the failure rate, denoted by $\lambda(t)$, and represents the probability per unit of time that the component will survive at $t + \Delta t$ since it already has survived for a time $t$. This variable is defined by [6, 14]

$$\lambda(t) = \lim_{\Delta t \to 0} \frac{f(t + \Delta t) - f(t)}{\Delta t} * \frac{1}{R(t)},$$
$$\lambda(t) = \frac{F'(t)}{R(t)} = \frac{f(t)}{1 - F(t)} = \frac{f(t)}{R(t)}, \tag{2}$$

where $f(t)$ is the density function up to time $t$ and $f(t + \Delta t)$ is the density function up to time $t + \Delta t$.

The failure rate is variable and depends on the time of use.

The failure rate has three stages, which are represented by the bathtub curve (Figure 1), and depicts the life of a component. This curve shows an early failure period during $t \in [0, t_1]$; this is caused by poor design and low-quality control. The random or constant failure period is defined by $t \in [t_1, t_2]$; this means that the failure may occur at any time during that period, due to poor operating conditions and variations on the installations. Finally, the wear failure period during $t \in [t_2, \infty]$ shows a failure rate increase which occurs at the end of the component useful life due to wear.

When the component has survived during a time $t \in [0, \infty]$, it is required to know the estimated average

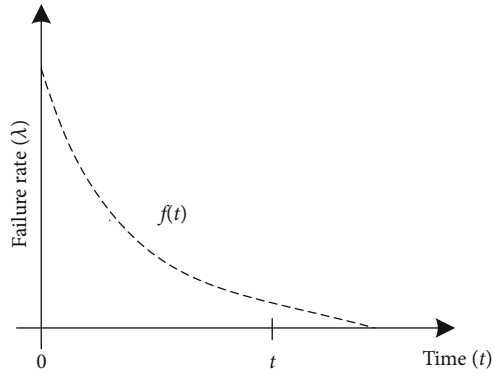


Figure 2: Density function $f(t)$ of a distribution $e(\lambda)$.

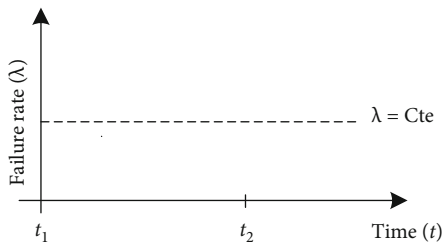


Figure 3: Constant failure rate of the exponential distribution.

value of lifetime before a fault occurs, known as the mean time between failures (MTBF) and is represented by [4, 6, 14]

$$\begin{aligned} \text{MTBF} &= \int_0^\infty t f(t)dt, \\ \text{MTBF} &= t \cdot R(t)\Big|_0^\infty + \int_0^\infty R(t)dt = \int_0^\infty R(t)dt. \end{aligned} \tag{3}$$

An exponential probability distribution is used in electronic components (Figure 2), since it represents a constant failure rate (Figure 3) for devices that have exceeded the initial time with greater results $t > 0$ and do not show wear failures.

The density function of the exponential distribution is represented by [4, 17]

$$f(t) = \lambda e^{-\lambda t}. \tag{4}$$

Integrating this equation in $t\epsilon[0, \infty]$ results in the cumulative distribution function of the exponential distribution:

$$F(t) = \int_0^t f(t)dt = -e^{-\lambda t}. \tag{5}$$

Substituting (5) into (1) obtained

$$R(t) = e^{-\lambda t}. \tag{6}$$

This equation is the exponential reliability function. To calculate the MTBF for the exponential distribution,

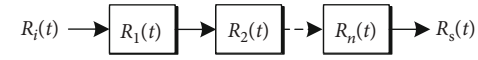


Figure 4: Reliability block diagram of a serial system.

(6) is substituted into (3) and is integrated, and results in [4, 6, 7, 12, 14]

$$\text{MTBF} = \int_0^\infty e^{-\lambda t}dt = \frac{1}{\lambda}. \tag{7}$$

*2.2. Reliability of a Serial System.* To facilitate the reliability analysis, it is done by dividing the system into subsystems. Each part of the system is represented by a block connected by arrows with other blocks of other related subsystems. Serial reliability (Figure 4) is the most practical in reliability analysis. It is said that a serial system will work properly if each block of each subsystem works as it should from $t$ up to $t + \Delta t$. A serial system has a catastrophic failure when any of its subsystems fail before finishing the process.

The reliability of a serial system $R_S(t)$ as the union of the probability of each subsystem (up to $n$) is represented by

$$R_S(t) = R_1(t) \cdot R_2(t), \cdots, R_n(t) = \prod_{i=1}^{n} R(t). \tag{8}$$

If an exponentially distributed independent system exists, (6) is used and is substituted into (8), obtaining the following:

$$R_S(t) = e^{-(\lambda_1+\lambda_2+\cdots+\lambda_n)t}, \tag{9}$$

where $\lambda$ is equal to

$$\lambda = \sum_{i=1}^{n} \lambda_i. \tag{10}$$

Substituting (10) into (7), the MTBF is obtained for a serial system; this is

$$\text{MTBF} = \frac{1}{\lambda} = \frac{1}{\sum_{i=1}^{n} \lambda_i}. \tag{11}$$

If the failure rate is constant in the subsystems, the following is obtained [6, 14, 17]:

$$\text{MTBF} = \frac{1}{\lambda} = \frac{1}{n\lambda_i}. \tag{12}$$

*2.3. Standard MIL HDBK217F.* The MIL HANDBOOK 217F standard is considered to make the reliability study of the photovoltaic system, which consists of the full-bridge inverter with an L or LCL coupling filter. The standard is a prediction tool based on statistical data on tests previously performed on the components. They contain data and operating specifications of the components, physical and mathematical models that help to predict and evaluate potential failures mainly of electronic equipment.

Table 1: Component stress model.

| Devices | Failure rate equation |
|---|---|
| Transistor | $\lambda_{PM} = \lambda_b(\pi_T \cdot \pi_A \cdot \pi_Q \cdot \pi_E)$ |
| Inductor | $\lambda_{PI} = \lambda_b(\pi_Q \cdot \pi_E \cdot \pi_T)$ |
| Capacitor | $\lambda_{PC} = \lambda_b(\pi_T \cdot \pi_C \cdot \pi_V \cdot \pi_{SR} \cdot \pi_Q \cdot \pi_E)$ |

Table 2: Arrhenius model.

| Devices | Temperature factor |
|---|---|
| Transistor | $\pi_T = \exp(-1925(1/T_j + 273 - 1/298))$ |
| Inductor | $\pi_T = \exp(-(0.11/0.00008617)(1/T_{HS} + 273 - 1/298))$ |
| Capacitor | $\pi_T = \exp(-(0.15/0.00008617)(1/T_a + 273 - 1/298))$ |

A model called component stress is used to obtain the analysis factors, such as component type, component quality, operating temperature, working environment, and component failure rate, among others. The mathematical model for the component stress analysis is [5, 12, 18]:

$$\lambda_P = \lambda_b(\pi_T \cdot \pi_S \cdot \pi_C \cdot \pi_Q \cdot \pi_E \cdot \pi_A \cdot \pi_{CV}), \quad (13)$$

where $\lambda_P$ is the failure rate of the component, $\lambda_b$ is the base failure rate of the component, $\pi_T$ is the encapsulation temperature factor, $\pi_S$ is the electrical stress factor, $\pi_C$ is the construction factor, $\pi_Q$ is the quality factor, $\pi_E$ is the environmental factor, $\pi_A$ is the application factor, and finally $\pi_{CV}$ is the capacitance factor.

In Table 1, the component stress models are shown for the elements that conform to the power stage, which are the transistor, inductor, and capacitor [5, 12, 16, 18].

As it can be observed in Table 1, the capacitor failure rate depends on the electrical stress factor $\pi_V$, which is a function of the stress voltage ($V_S$), and this is determined by [12]

$$V_S = \frac{V_a}{V_n}, \quad (14)$$

where $V_a$ is the applied voltage and $V_n$ is the nominal capacitor voltage.

It is noted that for all the component models, the failure rate depends directly on the temperature factor $\pi_T$, which indicates the acceleration ratio taking into account the previous temperature and the temperature in accelerated conditions (Table 2). And this is directly related to the power losses; for example, switching losses are calculated to obtain the junction temperature $T_j$, and this is calculated with [7, 12, 16]

$$T_j = T_C + (\theta_{jc} \cdot p_{loss}), \quad (15)$$

where $\theta_{jc}$ is the thermal resistance junction case, $P_{loss}$ is the switch losses, and $T_C$ is the case temperature.

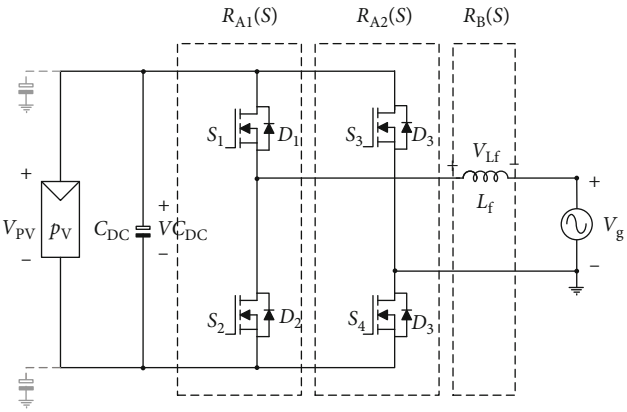


Figure 5: Full bridge with coupling L filter.

The MOSFET losses are determined by

$$P_{loss(static)} = R_{DSon} \cdot I_{rms}^2,$$
$$P_{loss(dynamic)} = V_{avg} \cdot I_{avg} \cdot (t_{on} + t_{off}) \cdot f_{sw}, \quad (16)$$
$$P_{loss} = P_{loss(static)} + P_{loss(dynamic)},$$

where $P_{loss}$ is the total losses, $R_{DSon}$ is the internal resistance, $I_{rms}$ represents the effective current, $I_{avg}$ and $V_{avg}$ are the average values, $t_{on} + t_{off}$ are the on and off times, and finally $f_{sw}$ is the switching frequency.

For the inductor, the hot spot temperature, $T_{HS}$, is used, and for the capacitor, the ambient temperature, $T_a$, is utilized [7, 12, 16, 18]:

$$T_{HS} = T_a + 1 \cdot 1\Delta T_d, \quad (17)$$

where $\Delta T_d$ is the ambient temperature change.

## 3. Power Stage and Design

The power stage considered is a full-bridge inverter, rated for 1 kW, and two alternatives of passive filters are analyzed. For case 1, an L filter is used (Figure 5) and, for case 2, an LCL filter (Figure 6).

The full-bridge inverter consists of two legs composed of two switches each one; they may be operated with bipolar or unipolar PWM modulation; MOSFETs were considered. In the paper, for both cases, a unipolar modulation is used. This type of modulation allows for greater efficiency and smaller filter size and value. Having a smaller filter will impact directly on losses, which will be lower, and then reliability will be bigger.

*3.1. Filter Design: Case 1.* For the L filter design, the inductor $L_f$ is considered a series inductance with a parasitic resistance. The L filter represents a first-order low-pass filter with a cutoff frequency of $\omega_L = R/L$ [19].

Resonance frequency $f_{res}$ is usually considered 10 times higher than the network frequency ($f_o$) and 10 times

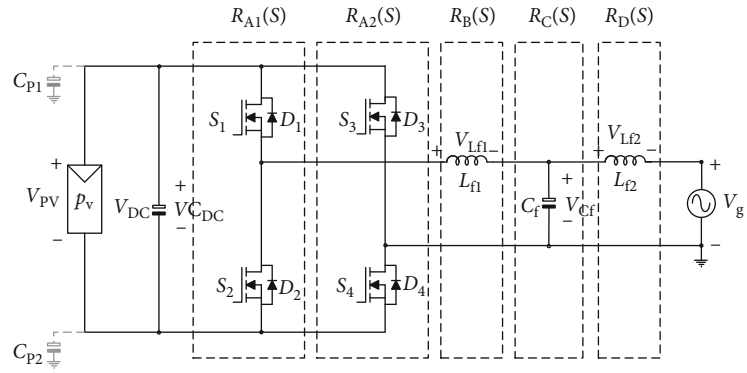


Figure 6: Full bridge with coupling LCL filter.

lower than the switching frequency ($f_{sw}$), as it is shown next:

$$10f_o \leq f_{res} \leq f_{sw}. \tag{18}$$

*3.2. Filter Design: Case 2.* For the design of the LCL filter, two inductors are considered ($L_{f1}$ and $L_{f2}$) and a capacitor.

The inverter output voltage is a function of the photovoltaic panel voltage $V_{pv}$ and the modulation index of the inverter $m$:

$$V_{C_f} = V_{pv}m. \tag{19}$$

The inverter operates with a unipolar modulation which results in lower filter size, and then considering the positive voltage of the inverter, the inductor $L_{f1}$ can be calculated by using [20]

$$L_{f1} = \frac{V_{pv}(1-m)m}{\Delta_{iL_{f1}} f_{sw}}, \tag{20}$$

where $\Delta_{iL_{f1}}$ is the current ripple in the inductor and $f_{sw}$ is the switching frequency.

To obtain $L_{f2}$, the next equation is used [8, 19]:

$$L_{f1} = \alpha L_{f2}, \tag{21}$$

where $\alpha$ is the ratio of the inductances.

The ratio $\alpha$ is selected between the interval $\alpha \in [3, 7]$. The capacitor is selected using (18) and considering $\omega_{res}$ as the resonant frequency, which is determined by [20, 21]:

$$C_f = \frac{L_{f1} + L_{f2}}{L_{f1}L_{f2}\omega_{res}}. \tag{22}$$

Table 3 shows the design parameters of the inverter and the filter, which were obtained using the previous equations.

*3.3. Reliability Design.* The reliability analysis is made for the system considering both filters. Then, considering first the full-bridge inverter with an L filter (Figure 5) and applying the serial reliability configuration (Figure 4), the reliability analysis can be performed by using equations (8), (9), (10), (11), and (12).

Table 3: Design parameters.

| L filter | LCL filter |
|---|---|
| $P_0 = 1$ kW | $P_0 = 1$ kW |
| $V_g = 127$ Vrms | $V_g = 127$ Vrms |
| $V_{pv} = 200$ V | $V_{pv} = 200$ V |
| $L_f = 2.4$ mH | $L_{f1} = 425\ \mu$H<br>$L_{f2} = 85\ \mu$H<br>$C_f = 9.9$ nF |

The reliability block diagram is shown in Figure 7(a), and it is the product of the reliability of the four switches and the inductor; this is

$$\begin{aligned} R_S(t) &= R_{A1}(t) \cdot R_{A2}(t) \cdot R_B(t), \\ R_{A1}(t) &= R_{S1}(t) \cdot R_{S2}(t), \\ R_{A2}(t) &= R_{S3}(t) \cdot R_{S4}(t), \\ R_B(t) &= R_{Lf}(t), \\ R_S(t) &= R_{S1}(t) \cdot R_{S2}(t) \cdot R_{S3}(t) \cdot R_{S4}(t) \cdot R_{Lf}(t). \end{aligned} \tag{23}$$

It is assumed that the reliability of the switches is $R_{S1}(t) = R_{S2}(t) = R_{S3}(t) = R_{S4}(t)$ equal; also, a constant failure rate is presented; therefore, $\lambda_{S1} = \lambda_{S2} = \lambda_{S3} = \lambda_{S4} = \lambda_1$; additionally, $\lambda_{Lf} = \lambda_2$ which represents the inductor failure rate.

Substituting the exponential reliability function (6) into (23) gives the total system reliability depending on the failure rate of each element, as shown next:

$$\begin{aligned} R_S(t) &= e^{-\lambda_1 t} \cdot e^{-\lambda_1 t} \cdot e^{-\lambda_1 t} \cdot e^{-\lambda_1 t} \cdot e^{-\lambda_2 t}, \\ R_S(t) &= e^{-(4\lambda_1 + \lambda_2)t}. \end{aligned} \tag{24}$$

To calculate the MTBF of the entire system, the total reliability is replaced, (24) in (3), and integrating from 0 to $t$,

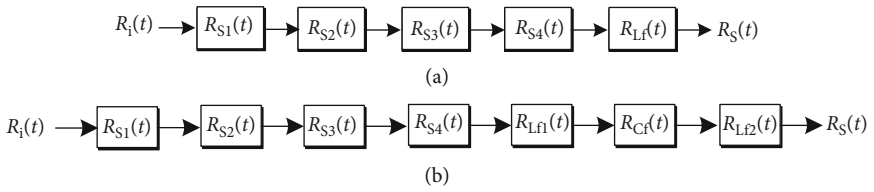


Figure 7: Serial block diagram of the full bridge with (a) L filter and (b) LCL filter.

when $t = \infty$. It can be seen that the MTBF is the inverse of the system failure rate:

$$\text{MTBF} = \frac{1}{4\lambda_1 + \lambda_2}. \tag{25}$$

The same process for the full-bridge inverter with the LCL filter (Figure 6) is performed. The reliability block diagram in series is shown in Figure 7(b), which represents the product of the reliability of each of the four switches, the two inductors, and the capacitor.

It is assumed also that $R_{S1}(t) = R_{S2}(t) = R_{S3}(t) = R_{S4}(t)$, and then the failure rate of the four switches is equal to $\lambda_{S1} = \lambda_{S2} = \lambda_{S3} = \lambda_{S4} = \lambda_1$; the inductor fault rate is $\lambda_{Lf1} = \lambda_2$ for the first one, $\lambda_{Lf2} = \lambda_3$ for the second, and finally $\lambda_{Cf} = \lambda_4$ for the capacitor. Based on the block diagram, the following is obtained:

$$\begin{aligned}
R_S(t) &= R_{A1}(t) \cdot R_{A2}(t) \cdot R_B(t) \cdot R_C(t) \cdot R_D(t),\\
R_{A1}(t) &= R_{S1}(t) \cdot R_{S2}(t),\\
R_{A2}(t) &= R_{S3}(t) \cdot R_{S4}(t),\\
R_B(t) &= R_{Lf1}(t),\\
R_C(t) &= R_{Cf}(t),\\
R_D(t) &= R_{Lf2}(t),\\
R_S(t) &= R_{S1}(t) \cdot R_{S2}(t) \cdot R_{S3}(t) \cdot R_{S4}(t) \cdot R_{Lf1}(t) \cdot R_{Cf}(t) \cdot R_{Lf2}(t).
\end{aligned} \tag{26}$$

The reliability of the full-bridge with the LCL filter is calculated as follows: (6) is substituted into (26) obtaining

$$\begin{aligned}
R_S(t) &= e^{-\lambda_1 t} \cdot e^{-\lambda_1 t} \cdot e^{-\lambda_1 t} \cdot e^{-\lambda_1 t} \cdot e^{-\lambda_2 t} \cdot e^{-\lambda_3 t} \cdot e^{-\lambda_4 t},\\
R_S(t) &= e^{-(4\lambda_1 + \lambda_2 + \lambda_3 + \lambda_4)t}.
\end{aligned} \tag{27}$$

Substituting (27) into (3), the MTBF of the entire system is calculated as

$$\text{MTBF} = \frac{1}{4\lambda_1 + \lambda_2 + \lambda_3 + \lambda_4}. \tag{28}$$

Equations (24), (25), (27), and (28) are used in the following section to calculate the reliability and the MTBF.

## 4. Reliability Analysis of the Photovoltaic System

To make the reliability analysis, some simulations are made, but also, some data are obtained from the standard. The simulation is performed to obtain the operating parameters; these are the voltage and current that are used in the reliability models. For the capacitor, the stress voltage ($V_S$) in used; on the other hand, the losses for the MOSFET ($P_{loss}$) must be calculated using the steady-state values of the converter.

*4.1. Numerical Simulation Results.* The numerical simulation of the full-bridge inverter for both cases, L and LCL filters, is performed with the design parameters of Table 3. PSIM® software is used for its versatility and simulation speed. Some parameters obtained from the datasheet were added to simulation components, such as MOSFET IRF540, to get the simulation results and reliability prediction closer to reality.

In Figure 8, the simulation for the power stage considering the L filter is observed. From top to bottom, the ac main voltage ($120\,V_{rms}$) and the injected current ($8.3\,A_{rms}$) are illustrated.

Figure 9 shows the results obtained for the LCL filter; from top to bottom, the ac main voltage ($120\,V_{rms}$) and the injected current under the same power conditions are graphed.

In both cases, the active power corresponds to 1 kW. The current is in phase with the ac voltage; therefore, a high power factor is achieved in both cases. The total harmonic distortion (THD) is different in both cases; Table 4 shows the THD of the injected current; it can be seen that values of 0.382% and 0.00926% for the L and LCL filters are obtained, respectively. According to the above, it is better to use an LCL filter than an L filter.

It is known that the distortion of the waveform affects the quality of the signal, therefore affecting directly the reliability.

*4.2. Reliability Calculation.* The numerical calculation of reliability is performed using the traditional MIL HDBK 217F standard. It is important to note that the reliability of the inverter depends on the acceleration parameter of the test and the temperature factor.

For the application of the standard, the adjustment factors are considered, also the base failure rate, which will generate an adjustment component failure rate. The total system failure rate, the MTBF, and the overall reliability are calculated. A high ambient temperature of 35°C is considered where the system will operate.

The adjustment factors used are shown in Tables 5 and 6 for the L and LCL filters, respectively, according to the

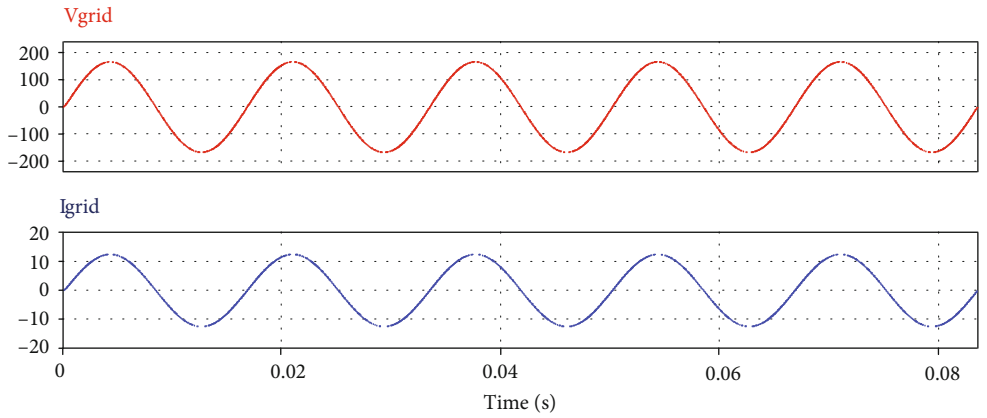


Figure 8: Active power injection filter with L filter. From top to bottom: average voltage (100 V/div) and average current (10 A/div).

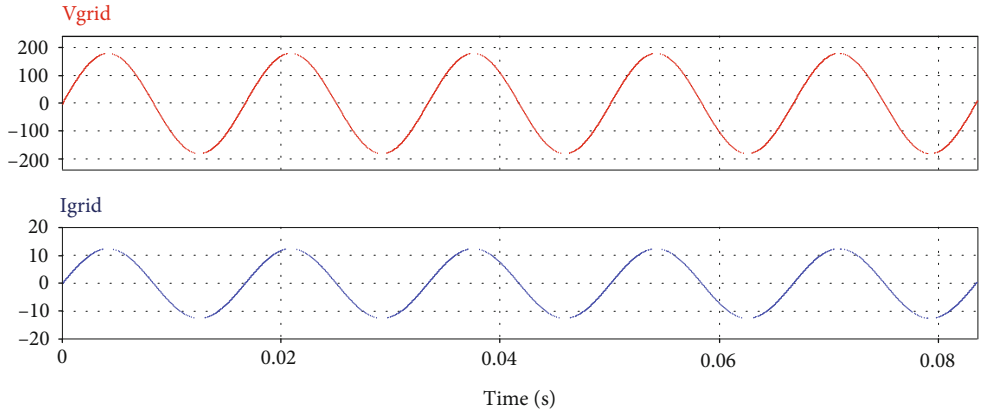


Figure 9: Active power injection filter with LCL. From top to bottom: average voltage (100 V/div) and average current (10 A/div).

Table 4: Filter L and LCL data and THD.

| | $L_{f1}$ | $C$ | $L_{f2}$ | THD |
|---|---|---|---|---|
| L filter | 2.56 mH | | | 0.382% |
| LCL filter | 425 $\mu$H | 9.9 $\mu$F | 85 $\mu$H | 0.00926% |

Table 5: L filter adjustment factors.

| Device | $\lambda_b$ | $\pi_T$ | $\pi_A$ | $\pi_Q$ | $\pi_E$ |
|---|---|---|---|---|---|
| MOSFET | 0.012 | 3.68 | 5.5 | 8 | 6 |
| Inductor | 0.00003 | 1.82 | | 3 | 6 |

Table 6: LCL filter adjustment factors.

| Device | $\lambda_b$ | $\pi_T$ | $\pi_A$ | $\pi_Q$ | $\pi_E$ | $\pi_C$ | $\pi_V$ |
|---|---|---|---|---|---|---|---|
| MOSFET | 0.012 | 3.67 | 5.5 | 8 | 6 | | |
| Inductor | 0.00003 | 1.82 | | 3 | 6 | | |
| Capacitor | 0.00037 | 1.209 | | 10 | 10 | 0.35449 | 26.17 |

Table 7: Reliability of L filter vs. LCL filter.

| Failure/$10^6$ | L | LCL |
|---|---|---|
| $\lambda_{PM}$ (MOSFET) | 12.973 | 12.800 |
| $\lambda_{PI}$ (Ls) | 0.00098350 | 0.00098355 |
| $\lambda_{PC}$ (C) | | 0.014092541 |
| $\lambda_{System}$ (total) | 51.173 | 51.216 |
| MTBF | 0.0195415 | 0.0195251 |

standard. The environmental factor is defined for the benign fixed terrestrial environment (GB) according to MIL HDBK 217.

The average and effective values of voltage and current are used for the calculation of losses, and these are made by using (16). The losses are used in the Arrhenius model to calculate the temperature factor $\pi_T$ that is necessary to obtain the MOSFET adjustment failure rate.

Table 7 shows the total system failure rate and the MTBF which are expressed in failure/$10^6$ hours. These were calculated using (24), (25), (27), and (28).

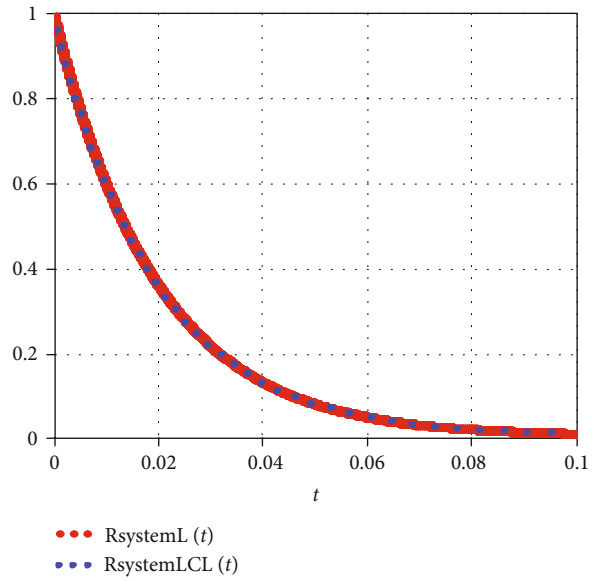


Figure 10: Comparison of the L and LCL filter reliability.

Table 8: Filter value vs. reliability.

| $L_{f1}$ | $\alpha$ | $L_{f2}$ | $C$ | $\lambda_{System}$ (failure/$10^6$hrs) | MTBF (failure/$10^6$hrs) | THD |
|---|---|---|---|---|---|---|
| 425 $\mu$H | 3 | 141 $\mu$H | 6.6 $\mu$F | 51.214 | 0.0195251 | 0.00910% |
| 425 $\mu$H | 4 | 106 $\mu$H | 8.2 $\mu$F | 51.215 | 0.0195251 | 0.00922% |
| 425 $\mu$H | 5 | 85 $\mu$H | 9.9 $\mu$F | 51.216 | 0.019525 | 0.00926% |
| 425 $\mu$H | 6 | 71 $\mu$H | 11 $\mu$F | 51.216 | 0.019525 | 0.00941% |
| 425 $\mu$H | 7 | 61 $\mu$H | 13 $\mu$F | 51.216 | 0.019525 | 0.00934% |

In the case of the full-bridge with an L filter, the MOSFETs contribute to 99.99% of the global failure rate and the inductor 0.01%. For the full-bridge with an LCL filter, again, the greater contribution for the global failure rate is given by the MOSFETs with 99.97%, while the inductors have 0.0038% and the capacitor with 0.0261%.

It is observed that the most susceptible element to fail is the MOSFET. The reliability prediction, with the MIL HDBK 217F standard, shows that a full-bridge inverter with an L filter is more reliable since the total failure rate of the full-bridge inverter with an LCL filter is higher ($\alpha = 5$); additionally, the same occurs with the MTBF, which determines the average life, and then it will be smaller. However, the reliability gain is marginal.

The decision-making, in this case, depends on the application. It should be noted that the number of elements plays a very important role in this calculation; the greater the number of the elements is, the higher the failure rate and the lower MTBF will be.

In Figure 10, the comparison of the L and LCL filter reliability is observed. The reliability is expressed in $10^6$ hrs. The dotted line represents the reliability of the LCL filter system with $0.0195251 \times 10^6$ hrs of life, while the straight line shows the L filter with $0.0195415 \times 10^6$ hrs.

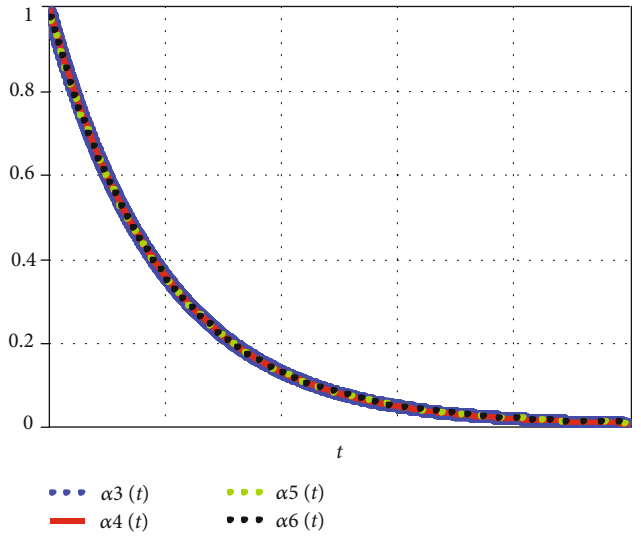


Figure 11: Comparison of reliability for different values of the components of the LCL filter.

The reliability difference in both cases is marginal. In the case of the LCL filter, the $\alpha$ ratio for the filter design also affects the reliability.

Table 9: L and LCL filter sizes.

| Filter type | | Value of the passive element | | | Passive element data | | | Total volume ($cm^3$) |
|---|---|---|---|---|---|---|---|---|
| | | $L_{f1}$ | $L_{f2}$ | $C$ | *Core* | *Core volume* | *Capacitor volume* | |
| L | | 2.4 mH | — | — | 3xETD-59 | 240.80 $cm^3$ | | 240.80 |
| LCL | $\alpha = 3$ | 425 $\mu$H | 141 $\mu$H | 6.6 $\mu$F | ETD-54<br>RM-14 | 56.8 $cm^3$<br>24.1 $cm^3$ | 12 $cm^3$ | 92.9 $cm^3$ |
| | $\alpha = 4$ | 425 $\mu$H | 106 $\mu$H | 8.2 $\mu$F | ETD-54<br>RM-12 | 56.8 $cm^3$<br>14.7 $cm^3$ | 12 $cm^3$ | 83.5 $cm^3$ |
| | $\alpha = 5$ | 425 $\mu$H | 85 $\mu$H | 9.9 $\mu$F | ETD-54<br>RM-12 | 56.8 $cm^3$<br>14.7 $cm^3$ | 16.12 $cm^3$ | 87.7 $cm^3$ |
| | $\alpha = 6$ | 425 $\mu$H | 71 $\mu$H | 11 $\mu$F | ETD-54<br>RM-12 | 56.8 $cm^3$<br>14.7 $cm^3$ | 16.12 $cm^3$ | 87.7 $cm^3$ |
| | $\alpha = 7$ | 425 $\mu$H | 61 $\mu$H | 13 $\mu$F | ETD-54<br>RM-12 | 56.8 $cm^3$<br>14.7 $cm^3$ | 20.83 $cm^3$ | 92.33 $cm^3$ |

In Table 8, a comparison for different values for the LCL filter is made, based on the $\alpha$ ratio of the filter design, which yields an effect on the reliability, MTBF, and THD. The best options are found for a ratio of three and four; with a ratio of three, a THD of 0.00910% and $0.0195251 \times 10^6$ hours of lifespan is obtained, with 51.214 failures/$10^6$ hrs. If the THD is smaller, the size of the second inductor increases and the capacitor value decreases, which in the end contributes to a lower failure rate increasing its useful life. As can be observed, the LCL filter with the $\alpha$ ratio of four has the same reliability with the L filter case.

In Figure 11, the comparison of the reliability for the LCL is observed; the graph is made using different values of $\alpha$.

Another important factor of the ratio $\alpha$ is the system size. Taking into account the inductor values of Table 8, the volume of the filter is calculated. In Table 9, due to the selected core and film capacitor, the volume is obtained; this is made for the L and LCL filter changing $\alpha$. As it can be observed, the best case for the volume is the LCL filter with a ration of four, since the size for the others is higher. It is important to notice that increasing the ratio $\alpha$ does not imply a lower volume since the cores available are finite; this may change depending on the rated power and type of cores used.

With this analysis, it can be deduced that the LCL filter may offer reliability compared to the L filter; therefore, the LCL filter should be always preferred because a better THD is obtained. If the volume is also added in the decision process, then, the ratio $\alpha$ must be selected properly and not necessarily high because the reliability shows that not only a lower $\alpha$ is better, but also the volume may not decrease by increasing $\alpha$.

## 5. Conclusion

In this article, the prediction of the reliability of a full-bridge inverter with different coupling filters is presented. The MIL HDBK 217 standard is used to calculate the failure rate and the mean time between failures. The study showed that the devices that are most likely to fail are the MOSFETs, due to thermal and electrical stresses that they are subjected during the switching stage.

The system with the L filter has an average life greater than the LCL filter usually designed, but marginal; however, the LCL case offers the best THD. Another analysis illustrates that the system reliability with LCL coupling is affected by the ratio $\alpha$, resulting in the fact that a value of 3 gets the best characteristic regarding THD and reliability, even comparable with the use of the L filter.

If the volume is considered, then the ratio $\alpha$ should be selected carefully since the higher ratio does not imply the lower volume according to the analysis; however, due to the reliability analysis and the THD obtained, the lower ratio $\alpha$ should be preferred. Then a compromise between reliability and volume can be made; the best case is a ratio of four in the analysis presented here.

## Data Availability

The data used to support the findings of this study are included within the article.

## Conflicts of Interest

The authors declare that there is no conflict of interest regarding the publication of this paper.

## Acknowledgments

This research was partially funded by the PROMINT-CM S2018/EMT-4366 program from the Comunidad de Madrid, Spain. Also, this work was partially funded by Tecnológico Nacional de México.

## References

[1] B. K. Bose, "Global warming: energy, environmental pollution, and the impact of power electronics," *IEEE Industrial Electronics Magazine*, vol. 4, no. 1, pp. 6–17, 2010.

[2] A. Chakraborty, "Advancements in power electronics and drives in interface with growing renewable energy resources," *Renewable and Sustainable Energy Reviews*, vol. 15, no. 4, pp. 1816–1827, 2011.

[3] N. Gupta, R. Garg, and P. Kumar, "Sensitivity and reliability models of a PV system connected to grid," *Renewable and Sustainable Energy Reviews*, vol. 69, pp. 188–196, 2017.

[4] A. Ristow, M. Begovic, A. Pregelj, and A. Rohatgi, "Development of a methodology for improving photovoltaic inverter reliability," *IEEE Transactions on Industrial Electronics*, vol. 55, no. 7, pp. 2581–2592, 2008.

[5] S. Harb and R. S. Balog, "Reliability of candidate photovoltaic module-integrated-inverter (PV-MII) topologies—a usage model approach," *IEEE Transactions on Power Electronics*, vol. 28, no. 6, pp. 3019–3027, 2013.

[6] F. Richardeau and T. T. L. Pham, "Reliability calculation of multilevel converters: theory and applications," *IEEE Transactions on Industrial Electronics*, vol. 60, no. 10, pp. 4225–4233, 2013.

[7] S. E. De León-Aldaco, H. Calleja, F. Chan, and H. R. Jiménez-Grajales, "Effect of the mission profile on the reliability of a power converter aimed at photovoltaic applications—a case study," *IEEE Transactions on Power Electronics*, vol. 28, no. 6, pp. 2998–3007, 2013.

[8] P. Channegowda and V. John, "Filter optimization for grid interactive voltage source inverters," *IEEE Transactions on Industrial Electronics*, vol. 57, no. 12, pp. 4106–4114, 2010.

[9] J. Wu, H. Jou, Y. Feng, W. Hsu, M. Huang, and W. Hou, "Novel circuit topology for three-phase active power filter," *IEEE Transactions on Power Delivery*, vol. 22, no. 1, pp. 444–449, 2007.

[10] V. V. S. Pradeep Kumar and B. G. Fernandes, "A fault-tolerant single-phase grid-connected inverter topology with enhanced reliability for solar PV applications," *IEEE Journal of Emerging and Selected Topics in Power Electronics*, vol. 5, no. 3, pp. 1254–1262, 2017.

[11] U. Choi, F. Blaabjerg, and K. Lee, "Reliability improvement of a T-type three-level inverter with fault-tolerant control strategy," *IEEE Transactions on Power Electronics*, vol. 30, no. 5, pp. 2660–2673, 2015.

[12] F. Chan and H. Calleja, "Reliability estimation of three single-phase topologies in grid-connected PV systems," *IEEE Transactions on Industrial Electronics*, vol. 58, no. 7, pp. 2683–2689, 2011.

[13] Y. Yang, H. Wang, and F. Blaabjerg, "Reliability assessment of transformerless PV inverters considering mission profiles," *International Journal of Photoenergy*, vol. 2015, Article ID 968269, 10 pages, 2015.

[14] Y. Song and B. Wang, "Survey on reliability of power electronic systems," *IEEE Transactions on Power Electronics*, vol. 28, no. 1, pp. 591–604, 2013.

[15] A. K. Barnes, J. C. Balda, and A. Escobar-Mejía, "A semi-Markov model for control of energy storage in utility grids and microgrids with PV generation," *IEEE Transactions on Sustainable Energy*, vol. 6, no. 2, pp. 546–556, 2015.

[16] F. H. Aghdam and M. Abapour, "Reliability and cost analysis of multistage boost converters connected to PV panels," *IEEE Journal of Photovoltaics*, vol. 6, no. 4, pp. 981–989, 2016.

[17] "IEEE recommended practice for the design of reliable industrial and commercial power systems," *IEEE Std 493-2007 (Revision of IEEE Std 493-1997)*, pp. 1–383, 2007.

[18] "Reliability prediction of electronic equipment," *Military Handbook 217F, US Department of Defense*, 1995, Notice 2, December 1991 (Superseding).

[19] Y. Noh, B. Choi, S. Lee, J. Eom, and C. Won, "An optimal method to design a trap-CL filter for a PV AC-module based on flyback inverter," *IEEE Transactions on Industry Applications*, vol. 52, no. 2, pp. 1632–1641, 2015.

[20] F. Liu, X. Zha, Y. Zhou, and S. Duan, "Design and research on parameter of LCL filter in three-phase grid-connected inverter," *2009 IEEE 6th International Power Electronics and Motion Control Conference*, pp. 2174–2177, 2009.

[21] S. Jayalath and M. Hanif, "Generalized LCL-filter design algorithm for grid-connected voltage-source inverter," *IEEE Transactions on Industrial Electronics*, vol. 64, no. 3, pp. 1905–1915, 2017.